



This paper is a part of the hereunder thematic dossier published in OGST Journal, Vol. 68, No. 2, pp. 187-396 and available online [here](#)

Cet article fait partie du dossier thématique ci-dessous publié dans la revue OGST, Vol. 68, n°2, pp. 187-396 et téléchargeable [ici](#)

DOSSIER Edited by/Sous la direction de : Jean-Charles de Hemptinne

## InMoTher 2012: Industrial Use of Molecular Thermodynamics InMoTher 2012 : Application industrielle de la thermodynamique moléculaire

Oil & Gas Science and Technology – Rev. IFP Energies nouvelles, Vol. 68 (2013), No. 2, pp. 187-396

Copyright © 2013, IFP Energies nouvelles

- 187 > Editorial
- 217 > *Improving the Modeling of Hydrogen Solubility in Heavy Oil Cuts Using an Augmented Grayson Streed (AGS) Approach*  
Modélisation améliorée de la solubilité de l'hydrogène dans des coupes lourdes par l'approche de *Grayson Streed Augmenté* (GSA)  
R. Torres, J.-C. de Hemptinne and I. Machin
- 235 > *Improving Group Contribution Methods by Distance Weighting*  
Amélioration de la méthode de contribution du groupe en pondérant la distance du groupe  
A. Zaitseva and V. Alopaeus
- 249 > *Numerical Investigation of an Absorption-Diffusion Cooling Machine Using  $C_3H_8/C_9H_{20}$  as Binary Working Fluid*  
Étude numérique d'une machine frigorifique à absorption-diffusion utilisant le couple  $C_3H_8/C_9H_{20}$   
H. Dardour, P. Cézac, J.-M. Reneaume, M. Bourouis and A. Bellagi
- 255 > *Thermodynamic Properties of 1:1 Salt Aqueous Solutions with the Electrolyte Equation of State*  
Propriétés thermophysiques des solutions aqueuses de sels 1:1 avec l'équation d'état de réseau pour électrolytes  
A. Zuber, R.F. Checoni, R. Mathew, J.P.L. Santos, F.W. Tavares and M. Castier
- 271 > *Influence of the Periodic Boundary Conditions on the Fluid Structure and on the Thermodynamic Properties Computed from the Molecular Simulations*  
Influence des conditions périodiques sur la structure et sur les propriétés thermodynamiques calculées à partir des simulations moléculaires  
J. Janeček
- 281 > *Comparison of Predicted pKa Values for Some Amino-Acids, Dipeptides and Tripeptides, Using COSMO-RS, ChemAxon and ACD/Labs Methods*  
Comparaison des valeurs de pKa de quelques acides aminés, dipeptides et tripeptides, prédites en utilisant les méthodes COSMO-RS, ChemAxon et ACD/Labs  
O. Toure, C.-G. Dussap and A. Lebert
- 299 > *Isotherms of Fluids in Native and Defective Zeolite and Alumino-Phosphate Crystals: Monte-Carlo Simulations with "On-the-Fly" ab initio Electrostatic Potential*  
Isothermes d'adsorption de fluides dans des zéolithes silicées et dans des cristaux aluminophosphatés : simulations de Monte-Carlo utilisant un potentiel électrostatique *ab initio*  
X. Rozanska, P. Ungerer, B. Leblanc and M. Yannourakou
- 309 > *Improving Molecular Simulation Models of Adsorption in Porous Materials: Interdependence between Domains*  
Amélioration des modèles d'adsorption dans les milieux poreux par simulation moléculaire : interdépendance entre les domaines  
J. Puibasset
- 319 > *Performance Analysis of Compositional and Modified Black-Oil Models For a Gas Lift Process*  
Analyse des performances de modèles black-oil pour le procédé d'extraction par injection de gaz  
M. Mahmudi and M. Taghi Sadeghi
- 331 > *Compositional Description of Three-Phase Flow Model in a Gas-Lifted Well with High Water-Cut*  
Description de la composition des trois phases du modèle de flux dans un puits utilisant la poussée de gaz avec des proportions d'eau élevées  
M. Mahmudi and M. Taghi Sadeghi
- 341 > *Energy Equation Derivation of the Oil-Gas Flow in Pipelines*  
Dérivation de l'équation d'énergie de l'écoulement huile-gaz dans des pipelines  
J.M. Duan, W. Wang, Y. Zhang, L.J. Zheng, H.S. Liu and J. Gong
- 355 > *The Effect of Hydrogen Sulfide Concentration on Gel as Water Shutoff Agent*  
Effet de la concentration en sulfure d'hydrogène sur un gel utilisé en tant qu'agent de traitement des venues d'eaux  
Q. You, L. Mu, Y. Wang and F. Zhao
- 363 > *Geology and Petroleum Systems of the Offshore Benin Basin (Benin)*  
Géologie et système pétrolier du bassin offshore du Bénin (Bénin)  
C. Kaki, G.A.F. d'Almeida, N. Yalo and S. Amelina
- 383 > *Geopressure and Trap Integrity Predictions from 3-D Seismic Data: Case Study of the Greater Ughelli Depobelt, Niger Delta*  
Pressions de pores et prévisions de l'intégrité des couvertures à partir de données sismiques 3D : le cas du grand sous-bassin d'Ughelli, Delta du Niger  
A.I. Opara, K.M. Onuoha, C. Anowai, N.N. Onu and R.O. Mbah

# Influence of the Periodic Boundary Conditions on the Fluid Structure and on the Thermodynamic Properties Computed from the Molecular Simulations

J. Janeček

ENSTA ParisTech, 828 Boulevard des Marechaux, 91762 Palaiseau Cedex, France  
e-mail: janecek@ensta.fr

## Résumé — Influence des conditions périodiques sur la structure et sur les propriétés thermodynamiques calculées à partir des simulations moléculaires

— Nous avons déterminé les contributions directionnelles de la fonction de distribution par paire du fluide de Lennard-Jones, par simulation moléculaire de Monte Carlo dans des boîtes cubiques de différentes tailles. L'approche de Pratt et Haan est utilisée pour analyser la distorsion de la structure de fluide causée par les conditions périodiques ; la théorie et les résultats de simulation sont en bon accord. Nous avons étudié la relation entre l'anisotropie des fonctions de corrélation et la dépendance vis-à-vis de la taille du système de l'énergie interne résiduelle et du facteur de compressibilité. Les effets de taille deviennent significatifs dans les systèmes dont la taille de la boîte est inférieure à 5 fois le diamètre des particules, en particulier si la longueur de la boîte est égale à un multiple non entier du diamètre moléculaire. Quand la température augmente, les effets de taille sur la structure du fluide et les propriétés thermodynamiques deviennent moins importants. La principale cause de la déformation de la structure réside dans les corrélations entre particules à courte portée, tandis que les interactions à longue portée n'ont pas d'influence. Les effets de taille du système affectent toutes les simulations atomistiques, y compris celles utilisant les interactions courtes portées et les simulations de dynamique moléculaire. Cependant, les systèmes simulés actuellement sont généralement de taille suffisamment grande, donc la taille finie n'engendre pas de problèmes, sauf pour la détermination des propriétés de surface par des simulations hétérogènes, qui sont sensibles à la dimension latérale de la boîte de simulation.

## Abstract — Influence of the Periodic Boundary Conditions on the Fluid Structure and on the Thermodynamic Properties Computed from the Molecular Simulations

— The components of pair distribution function in different directions with respect to the coordinate system defined by the simulation box are determined for Lennard-Jones fluid simulated using the Monte Carlo technique in cubic boxes of various size. The approach of Pratt and Haan is employed to analyze the distortion of isotropic fluid structure due to the periodic boundary conditions and qualitative agreement is found between the theoretical and simulated course of particular angular components of distribution function. The relation between the anisotropy of correlation functions and the system size dependency of residual energy and compressibility factor is analyzed. The finite size effects become significantly pronounced in systems with size lower than 5 particle diameters, especially if the length of the box-edge is equal to a non-integer multiple of molecular diameter. With increasing temperature the implicit finite size effects on fluid structure as well as on the thermodynamic properties become less important. The primary cause of the structure deformation lies in the short-range interparticle correlations and the

*long-range interactions are not important; therefore, the implicit finite size effects influence all kinds of atomistic simulations, including those using the interactions of finite range and in the molecular dynamics simulations. However, at present the simulated systems are usually of sufficiently large size and ignoring the implicit finite size does not lead to serious problems, except for the determination of surface properties using the inhomogeneous simulations which are more sensitive to the lateral dimension of simulation box.*

## INTRODUCTION

For a long time, the molecular simulations of fluids served dominantly as a tool which helped to validate the quality of theoretical models and to gain (qualitative) understanding of the behaviour of simulated systems at molecular level. The development of transferable force-fields based on interaction-site model together with the improvements in simulation methodology of phase equilibria enable to simulate the behaviour of real systems with acceptable predictability [1]. At present time, modules for atomistic simulations are included in several packages designed for use in industrial applications.

The first systematic attempts to develop transferable force fields date back to the 80's and they were aimed to comprehend biologically relevant problems [2–4]. Within the computational biochemistry, structural characteristic are in the centre of attention while the macroscopic thermodynamic properties are of secondary importance. With respect to the range of temperatures and pressures applied in chemical industry, several force-field sets were designed to describe the behaviour of various classes of organic substances at wide range of conditions [5–19]. Within the petrochemical applications, the molecular simulations became popular in order to predict the behaviour of systems at high pressures or systems containing unstable, hypothetical or dangerous compounds. The transferable force-fields were successfully applied to model various phenomena, *e.g.* high pressure VLE [20–22], gas solubility in liquids [23], adsorption of organic compounds in zeolites [24] and even interfacial [25–27] or transport properties [28] of fluid mixtures.

The Periodic Boundary Conditions (PBC) are the most popular technique to eliminate the surface effects and to mimic the infinite bulk phases in the computer simulations. The systems modeled using the PBC are affected by two different size dependencies, denoted as explicit and implicit finite size effects since the early days of computer simulations [29, 30]. The explicit finite size effects are caused by the suppression of density fluctuations in systems with fixed number of particles and thus they can be reduced by using the grandcanonical ensemble (in case of Monte Carlo simulations). The implicit finite size effects (called also periodic or anomalous error) have the origin in the symmetry break enforced by the periodic boundaries from spherical to cubic

symmetry (in the simplest case of simple fluid and cubic box). Using the language of cluster expansion, this effects are attributed to cluster integrals which are large enough to go beyond the periodic boundary.

Mandell [31] determined the orientationally dependent pair correlation function for Lennard-Jones fluid and used the Born–Green equation to analyze the influence of the periodic error on thermodynamic and structural properties. Special accent was put on the influence of the implicit finite size effects in the simulations of crystallization processes. Recently, Wittich and Deiters [32] analyzed the influence of box dimensions and shape on the crystallization of sodium iodide and found correlation between the box shape and the type of the resulting crystal lattice.

Using the supermolecule concept Pratt and Haan [33, 34] derived a practical approximation for angularly dependent pair distribution function which is based on the radial distribution function for infinite system. The comparison with the simulation data of Mandell [31] proved qualitative agreement of their theory. Later, Denton and Egelstaff [35] re-examined the Pratt and Haan approach for krypton-like fluid modeled by Aziz potential for three different sizes of simulation box. The main drawback of their work was the fact that they performed the comparison for segments of given polar angle  $\theta$  irrespective of azimuth (*i.e.* the correlation function averaged within a latitudinal segment) or conversely averaged for fixed azimuth  $\phi$  (*i.e.* within a volume element of the shape of a watermelon slice).

Kolafa [36] studied the influence of implicit finite size effects on thermodynamic properties of Lennard-Jones fluid using the molecular dynamics simulations and compared the simulated values of internal energy and compressibility factor with the values obtained by solving the Ornstein–Zernike (OZ) equation under periodic boundary conditions. The observed oscillatory dependence of simulated thermodynamic properties on the system size with the period equal approximately to the particle diameter was in agreement with the results obtained by solving the OZ relation. For hard sphere systems below the Fisher–Widom transition (*i.e.* with non-oscillating pair correlation function), monotonic increase of the pressure with system size was observed [37].

The system size dependency of surface tension obtained by inhomogeneous simulations represents a closely related phenomenon. Chen [38] observed a systematic decay of the surface tension values with the increase of the lateral size

of the simulation box. More detailed studies by Gonzalez-Melchor *et al.* [39] and Orea *et al.* [40] have shown that this dependency has in fact oscillatory character with the period again equal to the particle diameter and that the oscillatory system size dependency appears also in elongated boxes which contain no interface. In our recent studies [41, 42], we discussed the relation between the surface tension oscillations and the change of fluid structure due to the introduction of PBC. The variations of coexistence densities and vapour pressure with system size were also observed [41].

In this study, we focus on compressed Lennard-Jones liquid (single phase system) for which we simulate the values of pair distribution function in different directions with respect to the coordinate system defined by the edges of the simulation box. Up to our knowledge, this is the first time such data are published for systems of varying size. We also present a semi-quantitative link between the fluid structure affected by PBC and the system size dependent values of internal energy and pressure. In the following section, we briefly describe the employed methodology and in Section 2, the obtained results are presented and discussed.

## 1 SIMULATION DETAILS

We carried out NVT Monte Carlo (MC) simulations of Lennard-Jones fluid at two different points:  $T^* = 0.81$ ,  $\rho^* = 0.8645$  and  $T^* = 1.2$ ,  $\rho^* = 0.8$ . For each of these systems, we performed a set of runs with various number of particles and size of the cubic simulation box modified to keep the number density constant. The length of the edge of cubic simulation box ranged from  $L_x \approx 3\sigma$  to  $L_x = 10.0\sigma$ ; the particular values are listed in Tables 1 and 2. Because of brevity, we use in following text the values rounded to the closest 0.25-multiple of the  $\sigma$ -parameter of the Lennard-Jones (LJ) potential which is defined as:

$$u(r) = 4\epsilon \left[ \left( \frac{\sigma}{r} \right)^{12} - \left( \frac{\sigma}{r} \right)^6 \right] \quad (1)$$

where  $\sigma$  is the distance where the repulsive and attractive parts have equal value and  $\epsilon$  is the depth of the energy minima. We use the reduced temperature  $T^*$  and density  $\rho^*$  which are defined as  $T^* = k_B T / \epsilon$  and  $\rho^* = \rho \sigma^3$ ,  $k_B$  being the Boltzmann constant.

The starting configuration for each system was prepared by an equilibration of random configurations of  $N$  particles in the simulation box of corresponding size; the length of the equilibration phase was 50 000 MC cycles which corresponds to  $N \times 50\,000$  generated configurations. The sufficiency of the equilibration phase was attested by the check of the course of internal energy for every system. The production runs were 250 000 MC cycles long. For the intermolecular interactions spherical truncation at  $R_c = L_x/2$  was applied.

TABLE 1

The residual internal energy per one particle  $U^* = U/Nk_B T$  and the compressibility factor  $Z$  for LJ fluid at  $T^* = 0.81$  and  $\rho^* = 0.8645$  obtained by MC simulations in cubic boxes of different size. In the first three columns the box dimension  $L_x$ , cut-off radius  $R_c$  and number of particles  $N$  for particular systems are given. The subscript denotes the statistical uncertainty of the last digit, e.g.  $-7.97_1 = -7.97 \pm 0.01$

$L_x/\sigma$	$R_c/\sigma$	$N$	$U^*$	$Z$
2.98530	1.49265	23	$-7.97_1$	0.2 <sub>1</sub>
3.22511	1.61255	29	$-7.53_2$	1.78 <sub>7</sub>
3.49794	1.74897	37	$-7.46_2$	1.6 <sub>1</sub>
3.73378	1.86689	45	$-7.44_2$	1.8 <sub>1</sub>
3.99208	1.99604	55	$-7.55_2$	1.22 <sub>6</sub>
4.24222	2.12111	66	$-7.50_8$	1.65 <sub>7</sub>
4.48515	2.24257	78	$-7.56_7$	1.48 <sub>8</sub>
4.73886	2.36943	92	$-7.58_1$	1.36 <sub>6</sub>
4.99904	2.49952	108	$-7.57_2$	1.31 <sub>6</sub>
5.24866	2.62433	125	$-7.51_2$	1.63 <sub>4</sub>
5.48939	2.74469	143	$-7.52_2$	1.59 <sub>3</sub>
5.74592	2.87296	164	$-7.52_8$	1.57 <sub>2</sub>
5.99215	2.99608	186	$-7.53_3$	1.51 <sub>2</sub>
6.24941	3.12471	211	$-7.53_1$	1.57 <sub>2</sub>
6.49623	3.24811	237	$-7.54_2$	1.54 <sub>3</sub>
6.99588	3.49794	296	$-7.53_1$	1.56 <sub>3</sub>
7.49512	3.74756	364	$-7.53_2$	1.57 <sub>3</sub>
7.99624	3.99812	442	$-7.53_4$	1.56 <sub>2</sub>
10.0000	5.00000	864	$-7.53_4$	1.56 <sub>2</sub>

TABLE 2

The values of residual internal energy and compressibility factor for LJ fluid at  $T^* = 1.20$  and  $\rho^* = 0.8$  obtained by MC simulations in boxes of different size

$L_x/\sigma$	$R_c/\sigma$	$N$	$U^*$	$Z$
2.97196	1.48598	21	$-4.821_6$	0.72 <sub>4</sub>
3.23165	1.61583	27	$-4.567_8$	1.52 <sub>7</sub>
3.48977	1.74488	34	$-4.459_5$	1.92 <sub>4</sub>
3.74444	1.87222	42	$-4.410_7$	2.21 <sub>5</sub>
3.99479	1.99739	51	$-4.45_1$	2.05 <sub>4</sub>
4.24046	2.12023	61	$-4.463_2$	1.99 <sub>5</sub>
4.48141	2.24070	72	$-4.469_6$	2.05 <sub>4</sub>
4.73634	2.36817	85	$-4.487_5$	1.99 <sub>3</sub>
5.00000	2.50000	100	$-4.488_4$	1.92 <sub>3</sub>
5.23845	2.61922	115	$-4.470_6$	2.00 <sub>2</sub>
5.49862	2.74931	133	$-4.464_2$	2.05 <sub>3</sub>
5.74890	2.87445	152	$-4.465_3$	2.04 <sub>2</sub>
5.99073	2.99536	172	$-4.469_5$	2.02 <sub>2</sub>
6.24667	3.12333	195	$-4.469_2$	2.03 <sub>2</sub>
6.49309	3.24654	219	$-4.471_2$	2.03 <sub>1</sub>
6.99660	3.49830	274	$-4.471_3$	2.02 <sub>2</sub>
7.49629	3.74815	337	$-4.469_4$	2.04 <sub>2</sub>
7.99609	3.99805	409	$-4.469_3$	2.03 <sub>2</sub>
10.0000	5.00000	800	$-4.469_2$	2.04 <sub>1</sub>

During the simulation, the values of the internal energy per one particle  $U/N = \sum_{i<j} u_{ij}$  and the diagonal components of the virial tensor  $\Pi$ , were stored after every 10th finished MC cycle. The components of virial tensor were



determined as product of the position of a particle and the force acting on it by the particles within the cut-off sphere,  $\Pi_{\alpha\alpha} = \sum_i r_i^\alpha F_i^\alpha$ . The reduced values of energy and components of virial are defined with respect to  $k_B T$ :  $U^* = U/Nk_B T$  and  $\Pi_{xx}^* = \Pi_{xx}/k_B T$ . The compressibility factor is related with the diagonal components of virial tensor as:

$$Z = \frac{\Pi_{xx}^* + \Pi_{yy}^* + \Pi_{zz}^*}{3N} \quad (2)$$

The standard long range corrections assuming uniform particle distribution beyond the cut-off distance were added to the final values of the internal energies and compressibility factor after the simulation run:

$$U_{lrc}^* = \frac{8\pi\rho^*}{T^*} \left( \frac{1}{9R_c^{*9}} - \frac{1}{3R_c^{*3}} \right) \quad (3)$$

$$Z_{lrc} = \frac{16\pi\rho^*}{T^*} \left( \frac{2}{9R_c^{*9}} - \frac{1}{3R_c^{*3}} \right) \quad (4)$$

Thanks to using the NVT ensemble, there was no need to consider long-range corrections at single particle moves in the course of simulation.

In order to describe the fluid structure, we determined the values of angularly dependent pair distribution function,  $g(r, \theta, \phi)$ . With respect to the cubic symmetry, it is sufficient to consider only the intervals  $0 \leq \theta \leq \pi/2$  for the polar latitude  $\theta$  and  $0 \leq \phi \leq \pi/4$  for the azimuth  $\phi$ . The thickness of angular interval was the same for both angles,  $\Delta\theta = \Delta\phi = \pi/20$ , so the interval for polar angle was divided into 10 parts, that for azimuth into 5 parts. The grid size for the distance coordinate  $r$  was  $\Delta r = 0.01\sigma$ .

For the angularly dependent distribution functions, we use a simplified notation  $g_{i_0, j_\phi}(r)$  where  $i_0\Delta\theta$  and  $j_\phi\Delta\phi$  stand for the upper borders of the corresponding angular intervals. This notation reflects the fact that the angular intervals are quite wide compared to the fine division of the distance coordinate. The notation  $g_{2,1}(r)$  thus represents the distribution function in direction specified by angular borders  $\pi/20 \leq \theta < 2\pi/20$  and  $0 \leq \phi < \pi/20$ .

Any occurrence of a pair of particles with proper separation and with angles  $\theta$  and  $\phi$  falling into one of the angular segments has contributed to the matching histogram; at every measurement polar angles were determined for all three possible choices of the polar axis (*i.e.* with respect to axes  $x$ ,  $y$  and  $z$ ). The data for the pair distribution functions were collected after every 10th finished MC cycle.

## 2 RESULTS AND DISCUSSION

Figure 1 shows the effect of box dimension on the course of the function  $g_{1,1}(r)$ , *i.e.* the component of pair distribution function in a narrow angular interval in the direction of cartesian axes. In order to lower the noise and make the figures more clear, the presented curves were smoothed

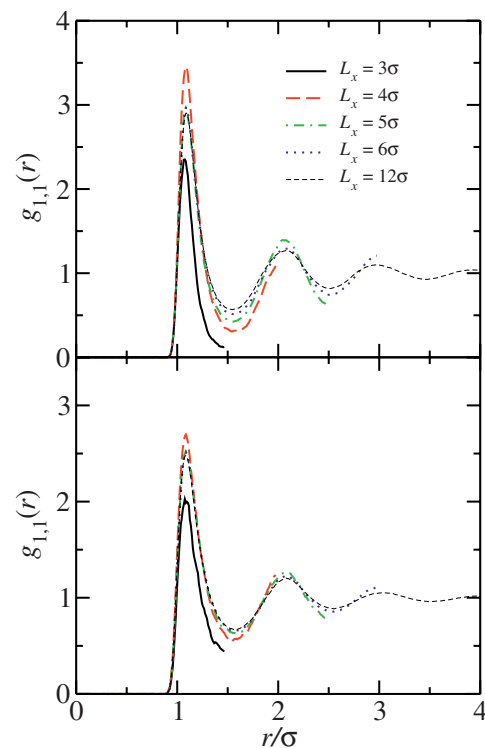


Figure 1

The course of  $g_{1,1}(r)$  obtained by MC simulations in systems with  $L_x = 3\sigma$  (solid black line),  $L_x = 4\sigma$  (dashed red),  $L_x = 5\sigma$  (dash-dotted green) and  $L_x = 6\sigma$  (dotted blue curve). The thin short-dashed black line shows the radial distribution function obtained in simulation box with dimension  $L_x = 12\sigma$ . The upper part shows the results for  $T^* = 0.81$  and  $\rho^* = 0.8645$ , the lower one for  $T^* = 1.2$  and  $\rho^* = 0.8$ .

by applying running average method calculated from three points (the scatter of raw distribution functions is demonstrated in Fig. 5, 6). The upper part shows the results obtained for  $T^* = 0.81$  and  $\rho^* = 0.8645$ , the lower one for  $T^* = 1.2$  and  $\rho^* = 0.8$ ; we follow this convention in all figures within this work.

The anisotropy of pair distribution function originates in the correlations between the particles within the basic simulation box and their images in the neighboring image boxes. The effect of the periodic error is thus most important close to the borders of the simulation box and that is why the deviations from the course of corresponding component obtained in “infinite” system are most pronounced in the smallest systems. For  $L_x = 3\sigma$  (solid black curve) and  $L_x = 4\sigma$  (long-dashed red curve), it even changes the height of the first maximum by more than 15 percent compared to the course of radial distribution function (rdf) simulated in box with  $L_x = 12\sigma$  (thin dashed line). In the case of the boxes of moderate size,  $L_x = 5\sigma$  (dash-dotted green line)

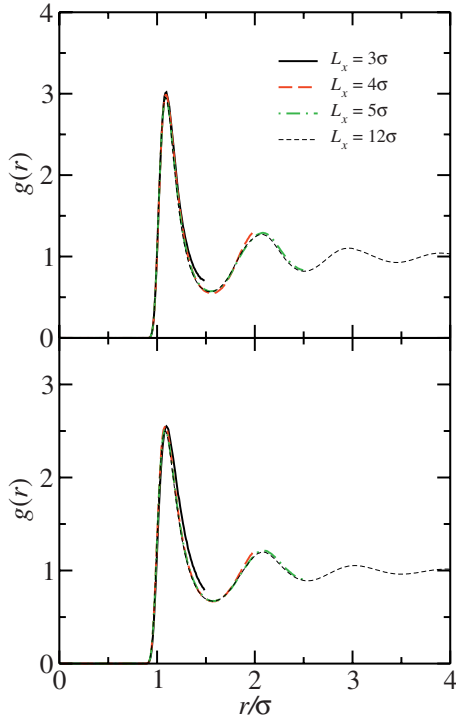


Figure 2

The course radial distribution function  $g(r)$  obtained by MC simulations in systems with  $L_x = 3\sigma$  (solid black line),  $L_x = 4\sigma$  (dashed red) and  $L_x = 5\sigma$  (dash-dotted green). The thin short-dashed black line shows the radial distribution function obtained in simulation box with dimension  $L_x = 12\sigma$ .

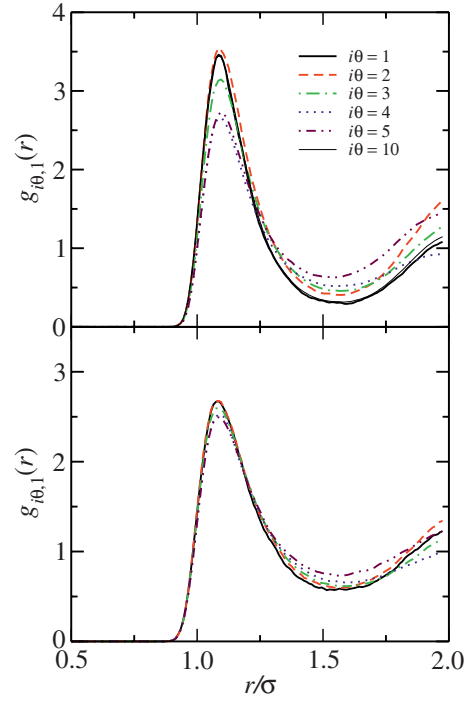


Figure 3

The course of the  $g_{i\theta,0}(r)$  components of pair distribution functions (*i.e.* in the  $xz$  plane) obtained in simulation box with  $L_x = 4\sigma$ . Different lines correspond to particular  $i\theta$  according to the inserted legend. The upper part again shows results for  $T^* = 0.81$  and  $\rho^* = 0.8645$ , the lower one for  $T^* = 1.2$  and  $\rho^* = 0.8$ .

and  $L_x = 6\sigma$  (dotted blue line), the deviations of  $g_{1,1}(r)$  from the course of rdf approve themselves at larger separations and they are less significant.

In Figure 2, we compare the course of radial distribution function  $g(r)$ , which represents the average of the pair distribution function  $g(r, \theta, \phi)$  over the angular variables:

$$g(r) = \frac{1}{4\pi} \int_0^\pi \int_0^{2\pi} g(r, \theta, \phi) \sin \theta d\theta d\phi \quad (5)$$

The results for the same system sizes as in Figure 1 are shown, only the results for  $L_x = 6\sigma$  are omitted because they fully coincide with the results for  $L_x = 12\sigma$ . Contrary to the particular components of pair distribution function, the rdf is considerably less sensitive to the system size. Its course at the region of the first maximum becomes independent of the system size (except the smallest system with  $L_x = 3\sigma$ ) and the deviations for separations approaching the half of box size do not exceed a few percent.

The variation of the pair distribution function in different directions for one box size is demonstrated in Figure 3 for

$L_x = 4\sigma$ . This figure shows the components of pair distribution function with varying latitude (polar angle  $\theta$ ) for fixed azimuthal segment at  $j_\phi = 1$ , *i.e.* in various directions in the  $xz$ -plane. The figure contains the only components with  $i_\theta \leq 5$ , since for  $j_\phi = 1$  it holds  $g_{i,1}(r) = g_{11-i,1}(r)$  as it is demonstrated by the curves for  $g_{1,1}(r)$  (thick solid black line) and  $g_{10,1}(r)$  (thin line) in the upper part of Figure 3.

The same set of functions obtained in simulation box with  $L_x = 4.5\sigma$  is displayed in Figure 4. One can see that relatively small change of box dimension can drastically affect the course of particular angular components of the pair distribution function. The order of functions according to their height at the first maximum as well as at the following minimum is almost completely reverted compared to the case with  $L_x = 4\sigma$ .

The prolate shape of the second maximum on  $g_{1,1}(r)$  in Figure 4 is a nice demonstration of the condition which has to be satisfied by the distribution function along the coordinate axes and which follows from the use of PBC, namely the requirement of the continuity of derivative at system boundaries,  $(\partial g_{1,1}(r)/\partial r)_{r=L_x/2} = 0$ . With respect to

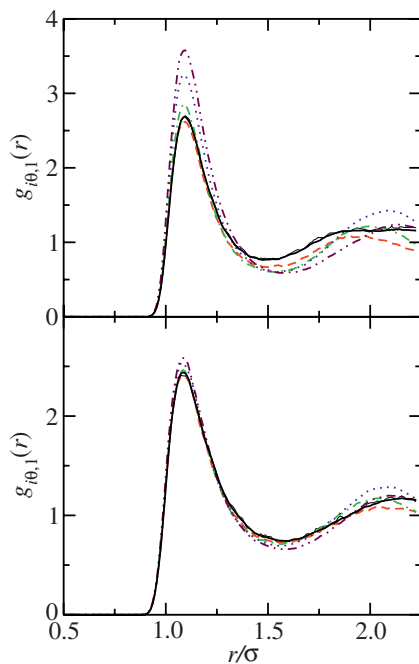


Figure 4

The same components of pair distribution function as plotted in Figure 3 obtained in box with  $L_x = 4.5\sigma$ . Different lines correspond to particular components in the same way as in Figure 3.

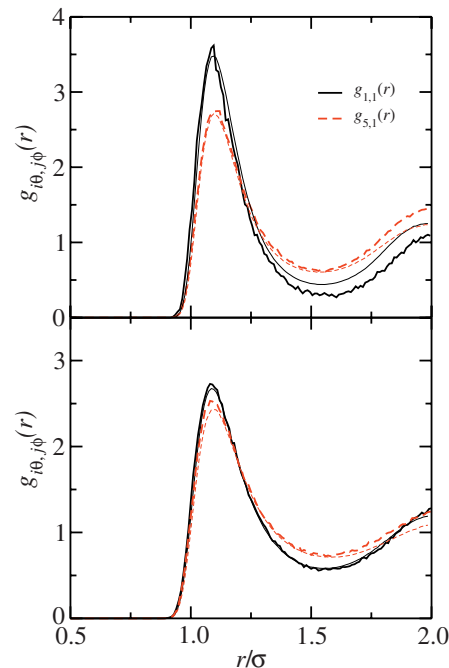


Figure 5

The comparison of simulated (thick curves) functions  $g_{1,1}(r)$  (solid black line) and  $g_{5,1}(r)$  (dashed red lines) with the first order prediction of Pratt and Haan (thin lines of corresponding colour and style) for  $L_x = 4.0$ .

the period of oscillations of rdf for the infinite system, this condition is easy to be satisfied in boxes with size equal to integer multiples of molecular diameter  $\sigma$ . For  $L_x = 4.5\sigma$ , this condition leads to the artificial elongation of second maximum and to large deviations from the course of infinite rdf.

Pratt and Haan suggested an approximation for the anisotropic pair distribution function which can be expressed as superposition of radial distribution functions:

$$g_{L_x}(\mathbf{r}_2 - \mathbf{r}_1) \approx g(r_{12}) \prod_i g(|\mathbf{r}_{2i} - \mathbf{r}_1|) \quad (6)$$

where  $g_{L_x}(\mathbf{r}_2 - \mathbf{r}_1)$  is the pair distribution function between points  $\mathbf{r}_1$  and  $\mathbf{r}_2$  inside the cubic box of size  $L_x$  and  $g(r)$  on the right-hand side represents the radial distribution function for the orientationally uniform LJ fluid (*i.e.* unaffected by periodic error) –  $g(r_{12})$  for particles 1 and 2 both in the basic box and  $g(|\mathbf{r}_{2i} - \mathbf{r}_1|)$  for particle 1 in the basic box and 2 in its  $i$ th image. We took the values of rdf simulated in box with  $L_x = 12\sigma$  for separations  $r \leq 6\sigma$ ; for larger distances, we used the WCA approximation [43] with the Boublík approximation of hard spheres rdf [44, 45]. We considered two shells of image boxes around the basic box, which means that 125 contributions were multiplied (including the central box).

In Figure 5, the functions  $g_{1,1}(r)$  (solid black line) and  $g_{5,1}(r)$  (red dashed) obtained in box with  $L_x = 4\sigma$  are compared with the prediction according to the Pratt and Haan approach (thin lines of corresponding color and type), analogous comparison for box with  $L_x = 4.5\sigma$  is shown in Figure 6. As mentioned in the first paragraph of this section, in these two figures the raw data are presented, that is why the simulated curves are more scattered compared to those in the remaining figures. In Figure 6, the symmetrically equivalent component  $g_{10,1}(r)$  is plotted instead of  $g_{1,1}(r)$ .

For  $L_x = 4\sigma$ , the superposition curves closely hit the simulated functions in the first maximum region and small deviations appear beyond the first minimum. While the component  $g_{1,1}(r)$  becomes overestimated, that for  $g_{5,1}(r)$  is undervalued in the region of first minimum. In the larger box with  $L_x = 4.5\sigma$ , strong deviations for the component  $g_{5,1}$  appear in the height of the first peak and between the minimum and borders of the box the approximate curve fits perfectly the simulated one. The deviations of the approximation of Pratt and Haan from simulated data seem to be slightly higher compared to those observed by Denton and Egelstaff [35]. This is probably caused by the fact that we compare pair distribution function in one direction while the previous authors used average integrated over one of the polar angles.

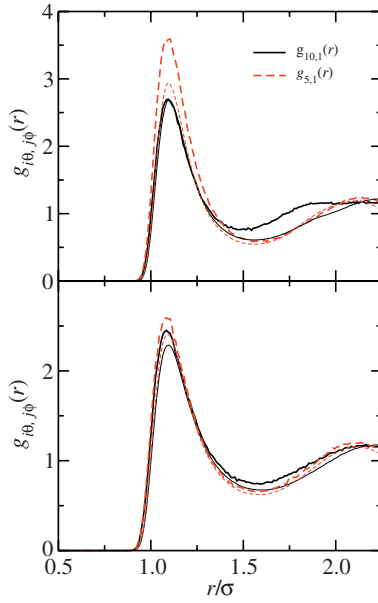


Figure 6

The same as in previous figure for results obtained in box with  $L_x = 4.5\sigma$ . Symmetrically equivalent components  $g_{10,1}(r)$  are shown instead of  $g_{1,1}(r)$ .

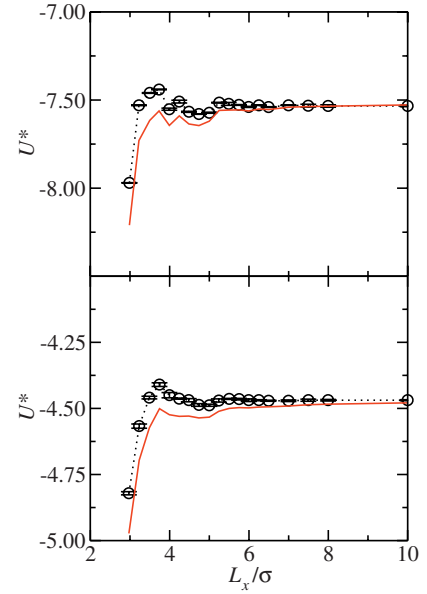


Figure 7

The dependence of simulated internal energy on the box dimension. The solid red lines show the values calculated from the simulated angularly dependent pair distribution function using the energy equation.

The energy and virial equations constitute the relation between the fluid structure and the basic thermodynamic properties – the residual internal energy and the compressibility factor. The angularly dependent versions can be written as:

$$U^* = \frac{\rho}{2k_B T} \int_{x=0}^{\infty} \int_{\theta=0}^{\pi} \int_{\phi=0}^{2\pi} u(x)g(x, \theta, \phi)x^2 dx \sin \theta d\theta d\phi \quad (7)$$

and:

$$Z = 1 - \frac{\rho}{6k_B T} \int_{x=0}^{\infty} \int_{\theta=0}^{\pi} \int_{\phi=0}^{2\pi} \frac{\partial u(x)}{\partial x} g(x, \theta, \phi) \times x^3 dx \sin \theta d\theta d\phi \quad (8)$$

We employed discrete forms of these equations to evaluate the internal energy and the compressibility factor of the systems simulated within this work and compared with the values obtained as system averages of the actual values during the course of simulation. Clearly, one can not expect that the ensemble average of a thermodynamic property will be different from the value calculated from the fluid structure. Our results only thus form nothing more than an explicit link between the system size dependency of thermodynamic properties (as was observed *e.g.* by Kolafa [36])

and the affected fluid structure (represented by the works of Mandell [31] or Denton and Egelstaff [35]).

In the liquid state, the residual internal energy is given by a sum of negative contributions (the probability of approaching two particles closer than  $r = \sigma$  is rather low), while the value of pressure consists of positive and negative contributions (due to the interactions of particles with separation smaller or larger than the minimum of Lennard-Jones potential at  $r_{min} = \sigma\sqrt[6]{2}$ ). Consequently, the values of pressure are affected by larger statistical error and the virial equation is rather sensitive to the employed integration scheme with respect to the distance variable  $r$ ; the difference between the values of compressibility factor obtained by the upper and lower rectangle methods is of order of units for the densities studied within this work. That is why we use the trapezoidal rule for  $r$  and middle rectangle method for the angular variables.

The comparison of the simulated values (*i.e.* the ensemble averages) with the values calculated from the (simulated) anisotropic pair distribution functions is shown in Figure 7 for the residual internal energy and in Figure 8 for the compressibility factor. Perfect agreement in the case of compressibility factor is slightly surprising compared to the acceptable but not perfect agreement observed for the values of residual internal energy with respect to the above



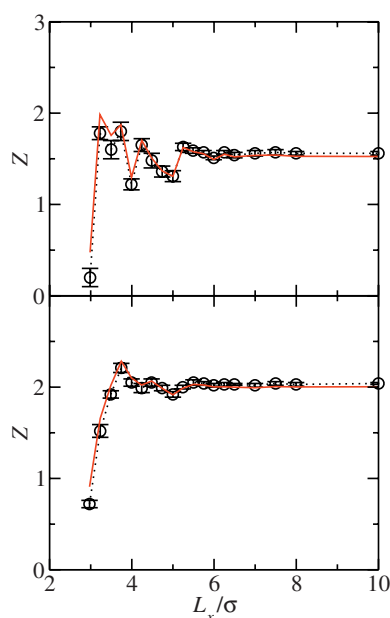


Figure 8

The dependence of simulated compressibility factor on the box dimension. The solid red lines show the values calculated from the simulated angularly dependent distribution functions using the virial equation.

mentioned sensitivity of the virial equation to the integration scheme and larger statistical errors. For both thermodynamic properties of interest, the system size dependency becomes negligible for simulation boxes with  $L_x \geq 6\sigma$ . This is in accordance with our previous study of the size dependency of vapor pressure and coexistence densities in inhomogeneous simulations [41].

## CONCLUSIONS

The use of the periodic boundary conditions changes the structure of simulated fluids and these modifications affect the thermodynamic properties of simulated system. Because of the origin in the correlations between particles in different image boxes, the implicit finite size effects are more manifested in smaller systems. For Lennard-Jones fluid slightly above the triple point (at  $T^* = 0.8$ ), we found that the effects on thermodynamic properties are sufficiently suppressed in boxes of size larger than  $6\sigma$  which corresponds to situation when the particle and its closest image are separated by five neighboring particles. At temperature close to the critical point ( $T^* = 1.2$ ), the effect of periodic error is lowered. Alejandre *et al.* [46] have demonstrated that for bulk fluid simulated in elongated tetragonal prism the increase of the softness of intermolecular potential makes the anisotropy of the stress tensor lower. Increased temperature has analogous effect as the increase of the softness of the potential – the probability of closer approaching of two particles

becomes higher and the fluid becomes more adaptable to the external conditions like the imposing of periodic boundary conditions.

Only very a small part of industrially important compounds can be described using simple spherically symmetric interactions, in most cases, the molecules must be modeled by the interaction site model, *i.e.* as a set of Lennard-Jones sites (eventually holding partial electric charges) connected by bonds. In such cases, the situation is more complex because of the anisotropy of the intermolecular interactions. For reasonably small and flexible molecules, we may hope that the simultaneous interaction of a central site and its images with other particles represents the leading contribution to implicit finite size effects, and consequently, we may expect disappearance of effect on thermodynamic properties in boxes larger than  $6 \times$  the Lennard-Jones diameter of the interaction site; this corresponds to 20–25 Å for compounds containing the most common groups. The situation might be less suitable when large rigid molecules (like *e.g.* aromatic compounds) are simulated. Also, the presence of strong directional interactions (typically the dipole moment) together with asymmetric shape has to be treated with special care. Atomistic simulations of the chain molecules with the length approaching or exceeding the box size represent separate problem.

It should be noted, that there are properties significantly more sensitive to structure deformations than is the residual internal energy or the pressure, *e.g.* the interfacial tension obtained using the inhomogeneous simulations. There are also reasons to believe that the effects on dynamical properties (like *e.g.* the diffusion coefficients or rotation autocorrelation functions) will be higher. To perform a system size check for each simulation is not accomplishable nor desirable but in some cases, this might be useful. In order to minimize the finite size effects, we recommend to choose the box dimensions in such a way, that the position of one of the maxima or minima on the rdf for the dominating pair of sites coincides with the borders of the box. On the other hand, to estimate the influence of finite size effects on studied property, it is useful to perform a comparative simulation in box of such size that  $g(r) = 1$  at the border. Also, the difference in the course of various components of pair distribution function can indicate the importance of implicit finite size effects for given system without the comparative simulation run. In cubic boxes, the component in the direction perpendicular to the wall ( $\theta = 0^\circ$ ,  $\phi = 0^\circ$ ), along the face diagonal ( $\theta = 45^\circ$ ,  $\phi = 0^\circ$ ) and along the space diagonal ( $\theta = 45^\circ$ ,  $\phi = 45^\circ$ ) are most suitable to give sufficient guidance.

## ACKNOWLEDGMENTS

The access to the MetaCentrum computing facilities provided under the research intent MSM6383917201 is highly

appreciated. We also thank to Dr. Patrice Paricaud for general support and to Jan Marek for many fruitful discussions.

## REFERENCES

- 1 Ungerer P., Lachet V., Tavitian B. (2006) *Oil Gas Sci. Technol.* **61**, 387-403.
- 2 Case D.A., Cheatham T.E., Darden T. *et al.* (2005) *J. Comput. Chem.* **26**, 1668-1688.
- 3 Van der Spoel D., Lindahl E., Hess B. *et al.* (2005) *J. Comput. Chem.* **26**, 1701-1718.
- 4 Jorgensen W.L., Tirado-Rives J. (2005) *J. Comput. Chem.* **26**, 1689-1700.
- 5 Toxvaerd S. (1990) *J. Chem. Phys.* **93**, 4290-4295.
- 6 Toxvaerd S. (1997) *J. Chem. Phys.* **107**, 5197-5204.
- 7 Smit B., Karaborni S., Siepmann J.I. (1995) *J. Chem. Phys.* **102**, 2126-2140.
- 8 Martin M.G., Siepmann J.I. (1998) *J. Phys. Chem. B* **102**, 2569-2577.
- 9 Martin M.G., Siepmann J.I. (1999) *J. Phys. Chem. B* **103**, 4508-4517.
- 10 Wick C.D., Martin M.G., Siepmann J.I. (2000) *J. Phys. Chem. B* **104**, 8008-8016.
- 11 Chen B., Potoff J.J., Siepmann J.I. (2001) *J. Phys. Chem. B* **105**, 3093-3104.
- 12 Nath S.K., Escobedo F.A., de Pablo J.J. (1998) *J. Chem. Phys.* **108**, 9905-9911.
- 13 Nath S.K., Banaszak B.J., de Pablo J.J. (2001) *J. Chem. Phys.* **114**, 3612-3616.
- 14 Nath S.K., Khare R. (2001) *J. Chem. Phys.* **115**, 10837-10844.
- 15 Ungerer P., Beauvais C., Delhommelle J., Boutin A., Rousseau B., Fuchs A.H. (2000) *J. Chem. Phys.* **112**, 5499-5510.
- 16 Pascual P., Ungerer P., Tavitian B., Pernot P., Boutin A. (2003) *Phys. Chem. Chem. Phys.* **5**, 3684-3693.
- 17 Ahunbay M.G., Perez-Pellitero J., Contreras-Camacho R.O., Teuler J.M., Ungerer P., Mackie A.D., Lachet V. (2005) *J. Phys. Chem. B* **109**, 2970-2976.
- 18 Boutard Y., Ungerer P., Teuler J.M., Ahunbay M.G., Sabater S.F., Perez-Pellitero J., Mackie A.D., Bourasseau E. (2005) *Fluid Phase Equilib.* **236**, 25-41.
- 19 Ungerer P. (2003) *Oil Gas Sci. Technol.* **58**, 271-297.
- 20 Economou I.G., Karakatsani E.K., Logotheti G.-E., Ramos J., Vanin A.A. (2008) *Oil Gas Sci. Technol.* **63**, 283-293.
- 21 Pérez-Pellitero J., Ungerer P., Mackie A.D. (2008) *Oil Gas Sci. Technol.* **63**, 277-282.
- 22 Elts E., Windmann T., Staak D., Vrabec J. (2012) *Fluid Phase Equilib.* **322**, 79-91.
- 23 Schnabel T., Vrabec J., Hasse H. (2005) *Fluid Phase Equilib.* **233**, 134-143.
- 24 Fuchs A.H., Boutin A., Teuler J.-M. Di Lella A., Wender A., Tavitian B., Ungerer P. (2006) *Oil Gas Sci. Technol.* **61**, 571-578.
- 25 Janeček J., Krienke H., Schmeer G. (2006) *J. Phys. Chem. B* **110**, 6916-6923.
- 26 Biscay F., Lachet V., Malfreyt P. (2011) *Actual Chim.* **358**, 19-23.
- 27 Neyt J.C., Wender A., Lachet V., Malfreyt P. (2012) *J. Phys. Chem. C* **116**, 10563-10572.
- 28 Lachet V., Creton B., de Bruin T., Bourasseau E., Desbiens N., Wilhelmssen O., Hammer M. (2012) *Fluid Phase Equilib.* **322**, 66-78.
- 29 Lebowitz J.L., Percus J.K. (1961) *Phys. Rev.* **124**, 1673-1681.
- 30 Lebowitz J.L., Percus J.K., Verlet L. (1967) *Phys. Rev.* **153**, 250-254.
- 31 Mandell M.J. (1976) *J. Stat. Phys.* **15**, 299-305.
- 32 Wittich B., Deiters U.K. (2010) *Molec. Simul.* **36**, 364-372.
- 33 Pratt L.R., Haan S.W. (1981) *J. Chem. Phys.* **74**, 1864-1872.
- 34 Pratt L.R., Haan S.W. (1981) *J. Chem. Phys.* **74**, 1873-1876.
- 35 Denton A.R., Egelstaff P.A. (1997) *Z. Phys. B* **103**, 343-349.
- 36 Kolafa J. (1992) *Molec. Phys.* **75**, 577-586.
- 37 Kolafa J., Labík S., Malijevský A. (2004) *Phys. Chem. Chem. Phys.* **6**, 2335-2340.
- 38 Chen L.-J. (1995) *J. Chem. Phys.* **103**, 10214.
- 39 Gonzalez-Melchor M., Orea P., Lopez-Lemus J., Alejandre J. (2005) *J. Chem. Phys.* **122**, 094503.
- 40 Orea P., Lopez-Lemus J., Alejandre J. (2005) *J. Chem. Phys.* **123**, 114702.
- 41 Janeček J. (2009) *J. Chem. Phys.* **131**, 124513.
- 42 Janeček J., Krienke H., Schmeer G. (2007) *Condens. Matter Phys.* **10**, 415-423.
- 43 Weeks J.D., Chandler D., Andersen H.C. (1971) *J. Chem. Phys.* **54**, 5237.
- 44 Boublík T. (1986) *Molec. Phys.* **59**, 775.
- 45 Šindelka M., Boublík T. (1997) *Fluid Phase Equilib.* **143**, 13-27.
- 46 Alejandre J., Bresme F., Gonzalez-Melchor M., del Rio F. (2007) *J. Chem. Phys.* **126**, 224511.

Final manuscript received in March 2012  
 Published online in March 2013

Copyright © 2013 IFP Energies nouvelles

Permission to make digital or hard copies of part or all of this work for personal or classroom use is granted without fee provided that copies are not made or distributed for profit or commercial advantage and that copies bear this notice and the full citation on the first page. Copyrights for components of this work owned by others than IFP Energies nouvelles must be honored. Abstracting with credit is permitted. To copy otherwise, to republish, to post on servers, or to redistribute to lists, requires prior specific permission and/or a fee: Request permission from Information Mission, IFP Energies nouvelles, fax. +33 1 47 52 70 96, or revueogst@ifpen.fr.